


Ferromagnetism of potassium metal under pressure loading into zeolite low-silica XShingo Araki,^{1,*} Nguyen Hoang Nam,² Kota Shimodo,³ Takehito Nakano,^{3,4} and Yasuo Nozue³¹*Department of Physics, Okayama University, Okayama 700-8530, Japan*²*Center for Materials Science, Faculty of Physics, Hanoi University of Science, Vietnam National University, 334 Nguyen Trai, Thanh Xuan, Hanoi, Vietnam*³*Department of Physics, Graduate School of Science, Osaka University, 1-1 Machikaneyama, Toyonaka, Osaka 560-0043, Japan*⁴*Institute of Quantum Beam Science, Graduate School of Science and Engineering, Ibaraki University, 2-1-1 Bunkyo, Mito, Ibaraki 310-8512, Japan* (Received 28 September 2018; revised manuscript received 4 January 2019; published 4 March 2019)

Potassium metal was loaded into K-form zeolite low-silica X (LSX) under the loading pressure P up to 1.5 GPa. A ferromagnetism is observed at $P \approx 0.9$ GPa below 13 K. The loading density of K atom n is estimated to be ≈ 15 per cage at the ferromagnetic loading pressure, and the pressure-derivative loading density dn/dP has a remarkable peak ≈ 11 GPa⁻¹ at $P \approx 0.95$ GPa. The density of states at the Fermi energy is estimated to be ≈ 46 states/eV per cage from the value of dn/dP on a simple model. The observed ferromagnetism is discussed in terms of the Stoner condition and the theory of the revised Rhodes-Wohlfarth plot.

DOI: [10.1103/PhysRevB.99.094403](https://doi.org/10.1103/PhysRevB.99.094403)**I. INTRODUCTION**

Alkali metals loaded into regular nanospaces (cages) of aluminosilicate zeolite crystals display novel electronic properties, such as a ferrimagnetism, a ferromagnetism, an antiferromagnetism, and an insulator-to-metal transition, etc. [1–16]. These properties are significantly different from those in the bulk form of alkali metals, and depend on the kind of alkali metals, their loading density, and the structure type of zeolite frameworks. In the present paper, we performed a pressure loading of K metal into K-form zeolite low-silica X (LSX), and observed a pure ferromagnetism at a specific loading density.

An outermost s electron of an alkali atom has a large size and a small binding energy, so that s electrons in bulk alkali metals are well described by the free-electron model. On the other hand, s electrons of alkali metals loaded into the regular cages of zeolites are confined by the potential of negatively charged aluminosilicate frameworks, and form clusters in cages by the sharing with several alkali-metal cations. These s electrons can be transferred to adjacent cages through shared windows. The first-principles band calculations revealed that the tight-binding approximation can be applied to s electrons of alkali metals in zeolites, if the size of the shared window is small enough and s electrons are well quantum-mechanically localized in cages [17,18]. A narrow energy band of s electrons with a strong s -electron correlation is expected in zeolites, because of the mutual Coulomb repulsion within cages [18].

Furthermore, s electrons have an interaction with the displacement of alkali cations distributed in cages of zeolites. Hence, s electrons have an electron-phonon deformation-potential interaction with alkali cations as well as the s -

electron correlation. Therefore, cation locations are stabilized by the interaction with the zeolite framework, s electrons, and other cations. s -electron wave functions are changed simultaneously by the configuration of cations, and vice versa. In order to take an overview of the electronic properties of alkali metals in zeolites, it is effective to introduce the following coarse-grained parameters of the correlated polaron system given by the so-called Holstein-Hubbard Hamiltonian [1,19,20]. The parameters are (1) a transfer energy t of an s electron between adjacent cages through windows due to the wave functions overlapping, (2) a Coulomb repulsion energy U (the Hubbard U) of two s electrons in the same cage, (3) the lattice relaxation energy by the short-range electron-phonon interaction S provided by the on-site interaction between the s electron and cation displacement in a cage, and (4) an average number of s electrons per cage n . A qualitative interpretation has been given for various properties of alkali metals in different zeolites by the t - U - S - n model [1], except for the quasi-low-dimensional systems, such as the quasi-one-dimensional metallic system in channel-type zeolite L [1,21,22]. The t - U - S - n model is effective for small- t systems, because of the applicability of the tight-binding approximation.

A. Zeolite low-silica X (LSX)

Zeolite crystals have regular nanospaces for guest materials, and different materials can be loaded there [1]. There are many different types of framework structures in zeolites [23]. In Fig. 1, the negatively charged aluminosilicate framework of zeolite low-silica X (LSX) is illustrated together with typical sites of exchangeable A cations [24]. The space group is $Fd\bar{3}$. In the present study, we used K-form LSX, namely, $A = \text{K}$. The framework structure type of zeolite LSX is FAU (IUPAC nomenclature [23]). β cages are arrayed in a diamond structure. Among β cages, supercages (cavities) of

*araki@science.okayama-u.ac.jp

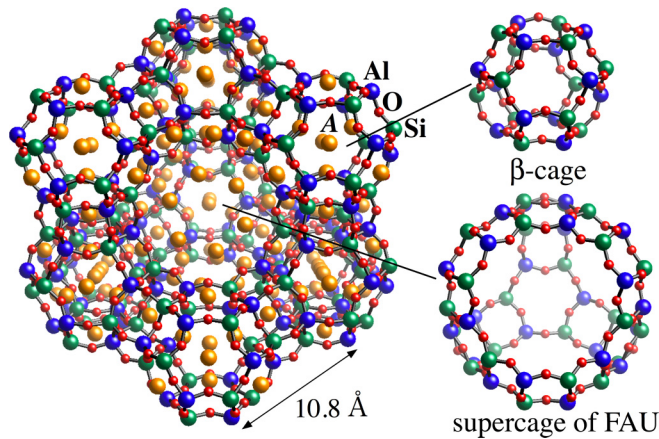


FIG. 1. Schematic illustrations of the aluminosilicate framework of zeolite low-silica X (LSX) and typical sites of A cations. The framework structure type is FAU. In the present study, we used K-form LSX, namely, $A = K$. The chemical formula before the loading of guest materials is given by $K_{12}Al_{12}Si_{12}O_{48}$ per β cage (or supercage of FAU), and abbreviated as K_{12} -LSX in the present paper. See also the polyhedral illustration of the structure in Fig. 2.

FAU are formed and also arrayed in a diamond structure. Hereafter, we call “supercage of FAU” simply by supercage. The chemical formula before the loading of guest materials is given by $K_{12}Al_{12}Si_{12}O_{48}$ per β cage (or supercage), and abbreviated as K_{12} -LSX in the present paper. This zeolite is a nonmagnetic insulator unless guest materials are loaded. In order to acquire an intuitive understanding of the framework structure, a polyhedral form is illustrated in Fig. 2. Each β cage has eight six-membered rings (6Rs), and is connected to four adjacent β cages by the sharing of hexagonal prisms [double six-membered rings (D6Rs)]. The inside diameter of

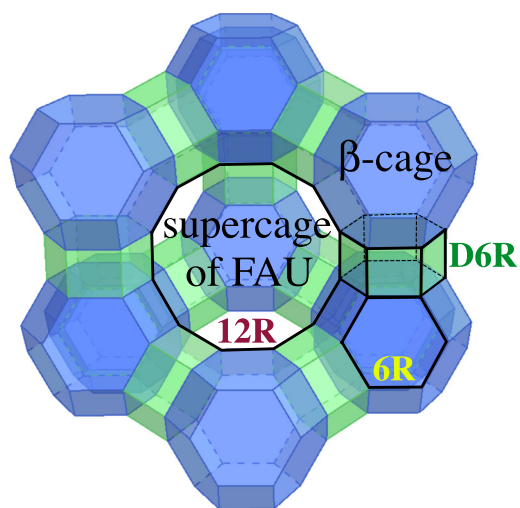


FIG. 2. Schematic illustrations of the framework polyhedra of zeolite LSX. Each β cage is connected to four adjacent β cages by the sharing of double six-membered rings (D6Rs), and arrayed in a diamond structure. Among the β cages, supercages of FAU are formed, and arrayed in a diamond structure by the sharing of 12-membered rings (12Rs).

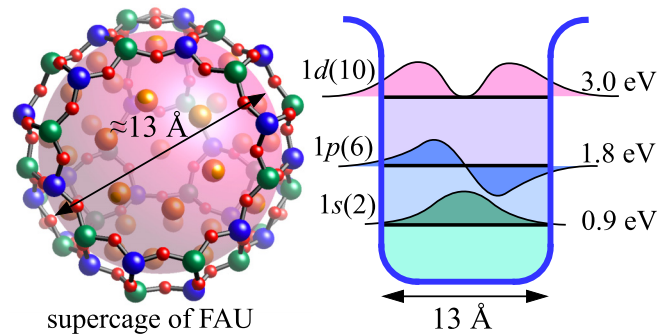


FIG. 3. Schematic illustrations of a K cluster in supercage of FAU and the quantum states of the s electron in the spherical quantum-well potential with the diameter of 13 \AA .

a β cage is $\approx 7 \text{ \AA}$. Supercages have the inside diameter of $\approx 13 \text{ \AA}$, and share windows of 12-membered rings (12Rs) with adjacent supercages. The inside diameter of a 12R is $\approx 8 \text{ \AA}$. Supercages and β cages share 6Rs with each other.

B. K-metal loading into zeolite K_{12} -LSX

In the present paper, we loaded guest K metal at n atoms per supercage (or β cage) into K_{12} -LSX, and describe it as K_n/K_{12} -LSX. There are two types of cages, supercage and β cage, in zeolite LSX. The value of n is defined by the chemical formula $K_n \cdot K_{12}Al_{12}Si_{12}O_{48}$, and is simply described as n per cage hereafter. The average number of s electrons is also n per cage. Cationic K clusters are formed in supercages and β cages, because s electrons are shared with both guest cations of K metal and zeolite cations, and are confined by the negatively charged framework.

Alkali metals are easily loaded into zeolite by the vapor phase for the unsaturated condition or by direct contact with the alkali metal for the saturated condition. Alkali atoms loaded into the surface area of zeolite crystals push other alkali atoms into deeper areas successively, and are distributed homogeneously. The s electrons successively occupy quantum states formed in cages. If we assume a spherical quantum well for cage, quantum states, such as $1s$, $1p$, and $1d$ states, are formed in increasing order of energy, and two, six, and ten s electrons can occupy respective quantum states successively [1]. A schematic illustration of clusters in supercage (supercage of FAU) and quantum states of an s electron in the spherical quantum well with the diameter of 13 \AA are given in Fig. 3. A large sphere in supercage is a schematic image of an s -electron wave function. $1s$, $1p$, and $1d$ quantum states have energies 0.9 , 1.8 , and 3.0 eV from the bottom of the quantum-well potential, respectively. The number within each parentheses indicates the degeneracy including spin. For example, $1s$ - $1p$ - $1d$ states can be filled totally with 18 s electrons of guest alkali metal. The spherical quantum-well potential, however, is primitive for supercage, because of large 8R windows. The spheres of s -electron wave functions in adjoining supercages largely overlap with each other, because the distance between adjoining supercages is 10.8 \AA , which is shorter than the diameter of supercage $\approx 13 \text{ \AA}$. Nevertheless, we use $1s$, $1p$, and $1d$ quantum states of the spherical quantum-well potential, because of a convenient

model to think about quantum states localized in a supercage. In zeolite A, K clusters are well localized in α cages, and the spherical quantum-well model well explains experimental results, because of narrow windows of α cages [1].

At lower loading densities, t is relatively small because s electrons occupy lower quantum states, and the electron-phonon interaction S dominates the system. Small polarons and small bipolarons are stabilized by the self-trapping of s electrons at $U > S$ and $U < S$, respectively [1]. An effective value of t for s electrons near Fermi energy is expected to increase with n , because s electrons occupy higher quantum states [1]. If we can increase n by the pressure loading, we can realize the s -electron occupation at much higher quantum states with larger t .

In ordinary materials, the average number of electrons doped in the common crystal structure is less than unity per site. In the alkali metal loading into zeolites, the average number of doped s electrons amounts to more than ten per cage with the same framework structure. Furthermore, alkali metals in zeolites can be changed or mixed with each other. We can make a widely systematic study of electronic states in alkali metals loaded in zeolites [1].

The loading density of alkali metal n for the unsaturated condition is adjusted by the weight ratio of alkali metal to zeolite in the sample preparation. In the case of the direct contact between a zeolite and an alkali metal, the Fermi energy of the zeolite sample coincides with that of the surrounding alkali metal. Under the pressure of zeolite samples embedded in alkali metal, an excess alkali metal can be loaded into the zeolite, and the Fermi energy increases. This pressure-loading technique was applied to the K system in zeolite A and the Na-K alloy system in zeolite LSX, and significant changes of paramagnetic and ferrimagnetic properties have been observed, respectively [9,10].

In K_n/K_{12} -LSX, n can be controlled continuously from 0 to 9 in unsaturated conditions [13]. At $n < 2$, samples are nearly nonmagnetic and insulating, because small bipolarons of K clusters are stabilized at supercages. The electrical resistivity suddenly decreases at $n = 6$ and a metallic phase is realized for $n > 6$ at the supercage network. Ferrimagnetic properties are observed at $n \approx 9$. Nonequivalent magnetic sublattices of K clusters are formed at β cages and supercages, and have an antiferromagnetic interaction with each other. A remarkable increase in the resistivity is observed at very low temperatures at $n \approx 9$, which is discussed in terms of the hypothesis of a Kondo-like insulator, where localized magnetic moments at β cages are distributed in a metallic narrow band of supercages [1,13].

In the present paper, samples of K_n/K_{12} -LSX were embedded in K metal and n was increased up to ≈ 17 under pressure. The ferrimagnetism at $n \approx 9$ disappears with the loading pressure, and a pure ferromagnetism is observed at ≈ 0.9 GPa corresponding to $n \approx 15$. The pressure-derivative loading density has a remarkable peak at the loading pressure where ferromagnetism appears. The peak is assigned to the high density of states of s electrons in K_n/K_{12} -LSX.

Up to now, nearly pure ferromagnetism has been observed in an insulating phase of $K_n/Na_{7.3}K_{4.7}$ -LSX for $8.4 < n < 9.7$, where the origin of magnetism is assigned to the ferromagnetic superexchange coupling between localized

magnetic moments of β -cage clusters via the sp^3 -like closed-shell clusters at supercages [16]. Ferromagnetic properties have been also observed in K clusters in zeolite A [2]. Although the observed ferromagnetic properties were initially assigned to the itinerant electron ferromagnetism [3], a spin-cant model of antiferromagnetism in a Mott insulator has been proposed after detailed studies [1,6,7]. On the other hand, the present ferromagnetic result in K_n/K_{12} -LSX at ≈ 0.9 GPa is an observation of itinerant electron ferromagnetism.

By the way, a ferromagnetism due to localized interstitial electrons has been expected in bulk potassium around ≈ 20 GPa according to the first-principles density-functional-theory calculations [25], and the compression has been demonstrated to push the valence band toward the strongly correlated electron regime [26]. The pressure of the present paper, however, is less than 2 GPa, and K cations are well separated as bulk K metal. Hence, bulk K metal set in a pressure cell for the pressure loading is in a Pauli paramagnetic phase.

II. EXPERIMENTAL PROCEDURES

A. Sample preparations and magnetic measurements

Zeolites are crystalline powders of a few microns in grain size. Sample preparation and magnetic measurements in the present study were done as follows. Zeolite K_{12} -LSX was fully dehydrated in vacuum at 500°C for 1 day. A distilled K metal was adsorbed into the K_{12} -LSX at 150°C , where the value of n was estimated from the weight ratio of K metal to K_{12} -LSX powder. We made a fully K-loaded sample, $K_{9.1}/K_{12}$ -LSX. We dispersed it in a distilled K metal, and prepared a drop of sample containing zeolite powder. We put it into a Teflon capsule in a dry-box filled with pure helium gas. The sealed Teflon capsule was set into a piston-cylinder-type pressure cell made of BeCu. Pressure was applied at room temperature by a piston made of WC with a hydraulic press. The change of inside volume and the pressure were obtained from the displacement of the piston and the force applied to the piston, respectively. The maximum pressure was 2 GPa. The pressure at room temperature was calibrated using the structural phase transitions of NH_4F at 0.365 GPa (I to II) and 1.17 GPa (II to III) [27].

Magnetic measurements were carried out using a superconducting quantum interference device (SQUID) magnetometer (Quantum Design, MPMS-XL). The background SQUID profile curve of the pressure cell was subtracted from that with a sample to detect the magnetization from the sample. The magnetization of the surrounding K metal is almost temperature independent and negligible in contrast to the value of K_n/K_{12} -LSX. A slight decrease in the pressure occurs at low temperatures, but we indicate the loading pressure at room temperature.

B. Measurements of loading density of potassium metal

We estimated the K-loading density n under pressure from the pressure dependence of the volume of the cell in which the zeolite sample and the surrounding K metal are set. When we apply the pressure on the cell, the change of cell volume is given by three terms: (1) the contraction of the surrounding

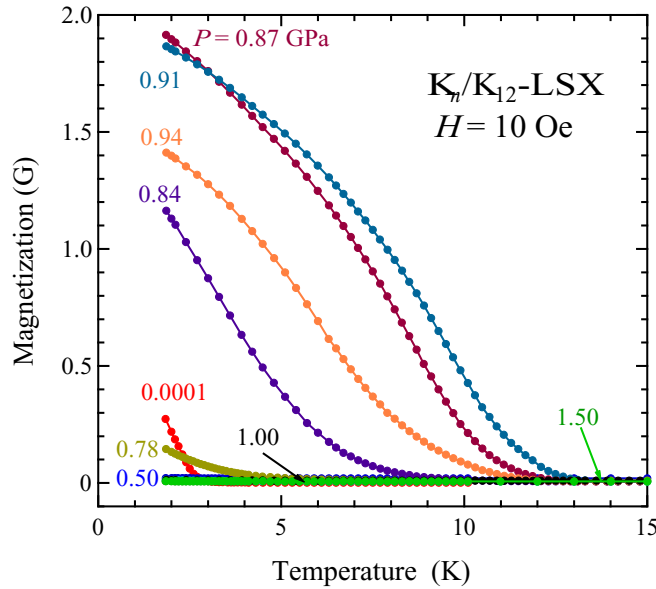


FIG. 4. Temperature dependence of magnetization under the magnetic field of 10 Oe at various K-loading pressures in K_n/K_{12} -LSX. The loading pressure P is indicated for each curve in units of GPa.

K metal, (2) the loading of the K metal into the zeolite, and (3) the deformation of the pressure cell. We measured the cell volume for various amounts of K metal without zeolite in advance to compensate the contributions of (1) and (3). We measured the decrease of cell volume step by step with increasing pressure, where we kept the pressure for 4 min for each step to achieve a stable pressure condition. The loading amount of K metal into zeolite in the step was estimated from the difference between the observed decrease and the decrease by the contributions of (1) and (3). The amount of the K loading into zeolite is subtracted from the amount of the surrounding K metal in the next step. We can estimate the differential K-loading density dn/dP at each step together with the decrease of the initial amount of the surrounding K metal. The contraction of the lattice constant of zeolite under the pressure loading was negligibly small, according to the x-ray diffraction experiment by using a diamond-anvil cell.

III. EXPERIMENTAL RESULTS AND DISCUSSIONS

A. Magnetic properties under pressure loading

The temperature dependence of magnetization M under the magnetic field $H = 10$ Oe at various K-loading pressures is shown in Fig. 4. The loading pressure P is indicated for each curve in units of GPa. At ambient pressure $P = 0.0001$ GPa, a ferrimagnetic magnetization [13] is seen below ≈ 3 K. With the increase in the loading pressure, the magnetization decreases and becomes paramagnetic at $P = 0.50$ GPa down to 1.8 K. At the loading pressure $P = 0.78$ GPa, a finite magnetization is seen at low temperatures, and quickly increases with the loading pressure. The magnetization has a peak value around 0.9 GPa. The magnetization quickly decreases with the loading pressure, and becomes again paramagnetic at $P = 1.00$ and 1.50 GPa.

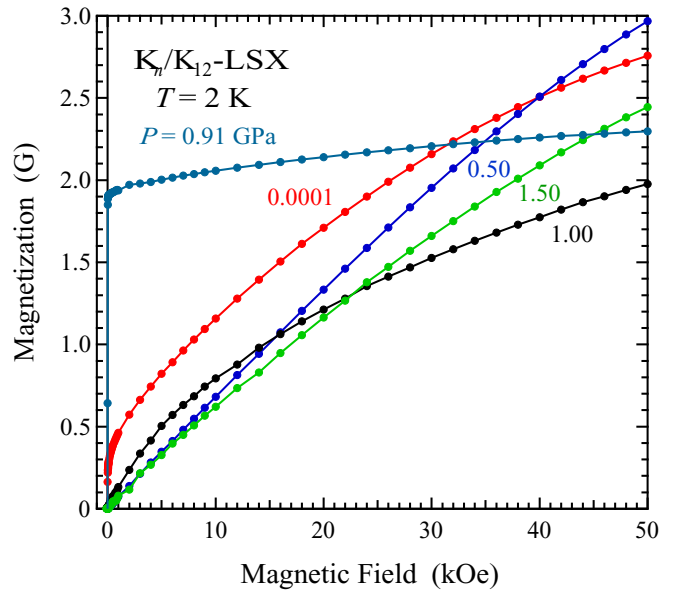


FIG. 5. Magnetic field dependence of magnetization at 2 K under the pressure loading of K metal in K_n/K_{12} -LSX. The loading pressure P is indicated for each curve in units of GPa.

The asymptotic Curie temperature at $P = 0.91$ GPa is estimated to be ≈ 13 K, and the Curie temperature estimated from the Arrott-plot analysis is ≈ 10.8 K, which is slightly lower than the asymptotic value. The spontaneous magnetization $M(T)$ at $T = 0$ K for $P = 0.91$ GPa is estimated to be 1.97 G by the following Bloch's law due to spin-wave fluctuations in a three-dimensional system:

$$M(T) = M(0)(1 - aT^{3/2}), \quad (1)$$

where a is the Bloch constant. The value of the spontaneous magnetization 1.97 G corresponds to the magnetic moment $0.42\mu_B$ per cage, where μ_B is the Bohr magneton.

The magnetic field dependence of magnetization at 2 K up to $H = 50$ kOe for various loading pressures is shown in Fig. 5. The loading pressure P is indicated for each curve in units of GPa. The magnetization M at 0.0001 GPa indicates a ferrimagnetic magnetization at low fields and gradually increases up to 2.7 G at 50 kOe. The magnetization at 0.5 GPa indicates a paramagnetic behavior at low fields and gradually increases up to 3 G at 50 kOe. The magnetization at 0.91 GPa indicates a ferromagnetic magnetization at low fields and reaches almost constant value ≈ 2.3 G at 50 kOe. The magnetization at 1.5 GPa indicates a paramagnetic behavior at low fields and gradually increases up to 2.4 G at 50 kOe.

The asymptotic Curie temperature T_C is obtained from the temperature dependence of magnetization at 10 Oe. The Weiss temperature T_W is obtained from the Curie-Weiss law of paramagnetic susceptibility. T_C and T_W are plotted in Fig. 6 as the function of the loading pressure as well as the loading density n for the unsaturated condition. A negative value of Weiss temperature indicates an antiferromagnetic interaction related to the ferrimagnetism. In samples for $8 \lesssim n$ and $P \lesssim 0.4$ GPa, ferrimagnetic properties are seen. In samples for $0.4 \text{ GPa} \lesssim P \lesssim 0.7$ GPa, paramagnetic properties are seen. In samples for $0.7 \text{ GPa} \lesssim P \lesssim 1.0$ GPa, the Weiss temperatures

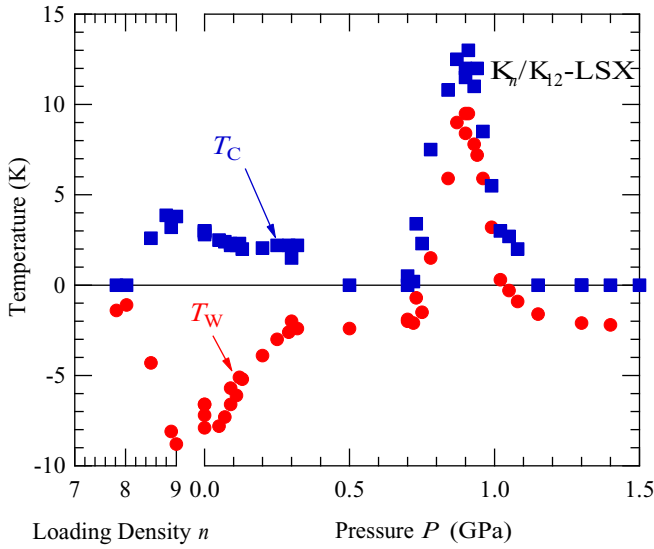


FIG. 6. Asymptotic Curie temperature T_C and Weiss temperature T_W in K_n/K_{12} -LSX as the functions of the loading pressure and the loading density n for the unsaturated condition.

are positive, and nearly pure ferromagnetism is observed. In samples for $1.0 \text{ GPa} \lesssim P$, paramagnetic properties are seen.

The Curie constant obtained from the Curie-Weiss law is plotted in Fig. 7 as the function of the loading pressure as well as the loading density n for the unsaturated condition. If we assume a localized spin $s = 1/2$ for each supercage, the Curie constant is calculated to be $3.17 \times 10^{-4} \text{ K emu/cm}^3$, as shown by the horizontal broken line in Fig. 7. The Curie constant for $8.5 \lesssim n$ and $P \lesssim 0.15 \text{ GPa}$ exceeds the above value. The Curie constant for samples of pressure loading basically decreases with the loading pressure. A quick decrease in the Curie constant with the loading pressure P is seen for $0 \text{ GPa} \lesssim P \lesssim 0.2 \text{ GPa}$ and $0.7 \text{ GPa} \lesssim P \lesssim 1 \text{ GPa}$. The Curie constant at $P = 0.91 \text{ GPa}$ is $\approx 1.28 \times 10^{-4} \text{ K emu/cm}^3$. This value corresponds to the effective local magnetic moment of $\approx 1.1 \mu_B$ per cage.

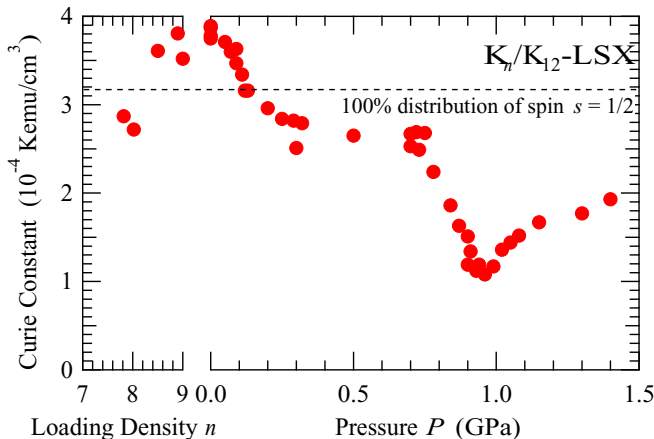


FIG. 7. Curie constant of K_n/K_{12} -LSX as the functions of the loading pressure P and the loading density n for the unsaturated condition.

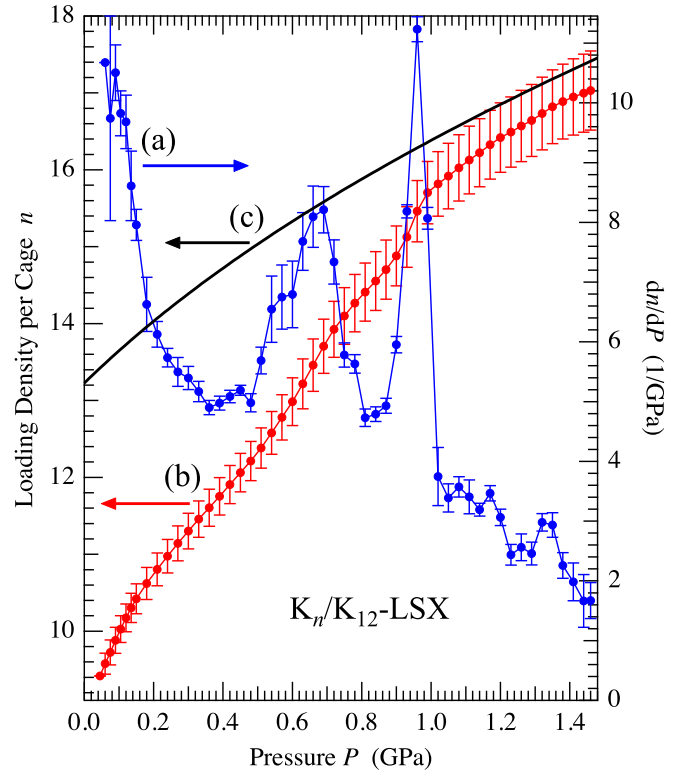


FIG. 8. Loading density of K atoms per cage in K_n/K_{12} -LSX at room temperature under the pressure P : (a) the differential loading density dn/dP , (b) the integral loading density n , and (c) the calculated number density of K atoms of bulk K metal per corresponding free space of cage in zeolite LSX.

B. Loading density of potassium metal

The differential K-loading density dn/dP is measured for each step of pressure loading at room temperature up to $P = 1.5 \text{ GPa}$, as shown in Fig. 8(a). There appear several peaks. The loading density n is obtained by the integral of dn/dP , as shown in Fig. 8(b), where the initial value of n at ambient pressure is 9.1 per cage.

The free volume ratio of zeolite LSX is roughly estimated to be about 50%. There are eight cages (supercages or β cages) in the unit cell of zeolite LSX, and the lattice constant is $\approx 25 \text{ \AA}$. The free volume per cage is estimated to be 50% of $1/8$ unit-cell volume, $0.5 \times 25^3/8 \text{ \AA}^3 (\approx 977 \text{ \AA}^3)$. A simple estimation of the K-atom number per the free volume under pressure is given in Fig. 8(c), where the density of bulk K metal is calculated by the third-order Birch-Murnaghan equation of state (or the first-order Birch equation of state) [28] given by

$$P(V) = \frac{3B_0}{2} \left[\left(\frac{V_0}{V} \right)^{7/3} - \left(\frac{V_0}{V} \right)^{5/3} \right] \times \left\{ 1 + \frac{3}{4} (B'_0 - 4) \left[\left(\frac{V_0}{V} \right)^{2/3} - 1 \right] \right\}. \quad (2)$$

P , V , and V_0 are the pressure, the volume at P , and that at $P = 0$, respectively. B_0 and B'_0 are the bulk modulus and its first pressure derivative, respectively. B_0 and B'_0 for potassium

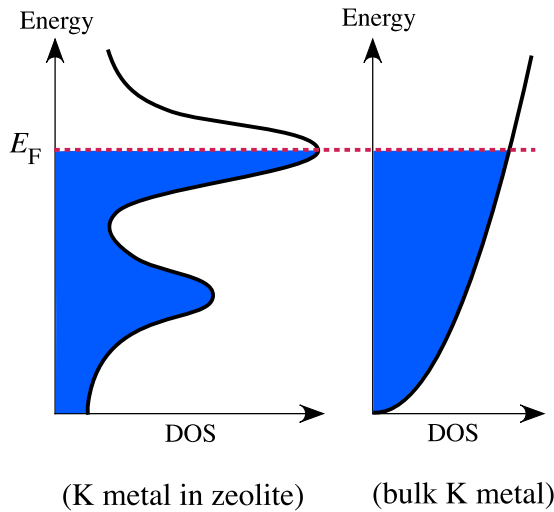


FIG. 9. Schematic illustration of the DOS of s electrons in zeolite and that of bulk K metal under pressure. They have a common Fermi energy E_F . The Fermi energy increases with the applied pressure.

metal are given as [28]

$$B_0 = 2.99 \pm 0.02 \text{ GPa},$$

$$B'_0 = 4.15 \pm 0.10.$$

The value of V_0/V is 1.4 ($V = 0.71V_0$) at $P = 2$ GPa. The contribution of B'_0 is very small at pressures less than 2 GPa.

The loading density $n = 9.1$ at ambient pressure is much lower than the expected value, 13.2, of bulk K metal for free space of zeolite LSX, as shown in Figs. 8(b) and 8(c). With the increase in the loading pressure, the loading density increases quickly, and approaches the maximum values for bulk K metal at $P \gtrsim 1$ GPa. K metal is very soft, and the size of the 12R windows of supercages shown in Fig. 2, ≈ 8 Å, is much larger than the size of the K atoms. Then, K_n/K_{12} -LSX embedded in the surrounding K metal smoothly accepts an excess K metal into the nanospaces under pressure. Actually, the lattice constant under the pressure of the K metal scarcely contracts, indicating that the zeolite framework does not feel stress from pressure. This condition may realize the K-atom loading (namely, the codoping of K cations and s electrons), and may keep the neutrality of the K-loaded zeolite. Under the equilibrium of loading, the Fermi energy of s electrons in the surrounding K metal and K_n/K_{12} -LSX coincide with each other at the direct contact condition, as illustrated schematically for the density of states (DOS) in Fig. 9. The Fermi energy E_F increases with the applied pressure.

According to the theoretical calculation of the energy band of bulk K metal under pressure, the bottom of the 4s-electron band has almost no shift in energy under lower pressures ($V > 0.6V_0$) [29], because the long-range Coulomb interactions between electrons and cations are almost canceled in monovalent metals [30,31]. According to the free-electron model, the E_F of the K metal measured from the bottom of the 4s-electron band is given by

$$E_F = \frac{\hbar^2}{2m} (3\pi^2 \rho)^{2/3}, \quad (3)$$

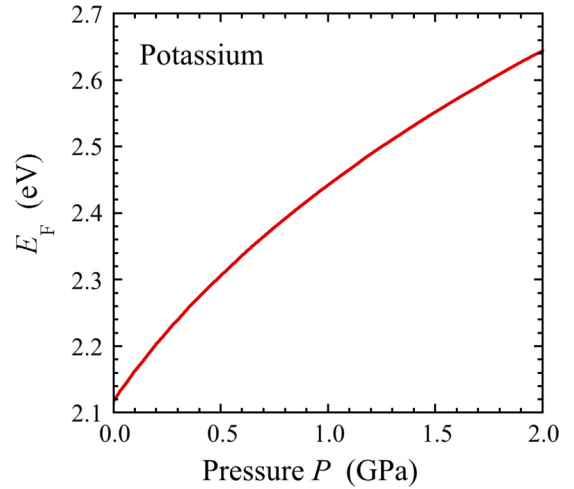


FIG. 10. The Fermi energy E_F of bulk K metal based on the free-electron model in Eq. (3) as the function of pressure $P(V)$ given by Eq. (2).

where the electron density ρ is given by

$$\rho = \rho_0 \frac{V_0}{V}. \quad (4)$$

ρ_0 is the electron density at ambient pressure, and given as $\rho_0 = 1.40 \times 10^{28} \text{ m}^{-3}$ in bulk K metal. In Fig. 10, the Fermi energy of the K metal in Eq. (3) is plotted as a function of pressure given by Eq. (2). The slopes around $P = 0, 0.7$, and 0.96 GPa are $\approx 0.5, \approx 0.29$, and ≈ 0.24 eV/GPa, respectively. The differential loading densities around $P = 0, 0.7$, and 0.96 GPa in Fig. 8(a) are $\approx 10, \approx 8$, and ≈ 11 GPa $^{-1}$, respectively. These values correspond to the DOS per cage, $\approx 20, \approx 28$, and ≈ 46 states/eV, respectively. The DOS of bulk K metal at the Fermi energy is ≈ 10 states/eV per $0.5 \times 25^3/8$ Å 3 (which is the free volume of cage in zeolite LSX). The estimated DOS at 0.96 GPa in K_n/K_{12} -LSX, ≈ 46 states/eV, seems to be large enough to consider the ferromagnetic phase transition at low temperatures, as discussed later. The full widths of peaks at 0.7 and 0.96 GPa in Fig. 8(a) are ≈ 0.4 and ≈ 0.15 GPa, respectively. They correspond to the energy bandwidths of ≈ 0.1 and ≈ 0.04 eV, respectively. In an accurate model, we need to consider a slight energy shift of the DOS of K metal in zeolite under pressure, but we neglect it here for simplicity.

C. Discussions on magnetic properties

As explained in Sect. IB, the simplest model of quantum states in the zeolite cage is given by the spherical quantum-well potential [1]. The $1s, 1p$, and $1d$ states are formed, and two, six, and ten s electrons can occupy respective states. According to this primitive model, energies of $1s, 1p$, and $1d$ states with the diameter of supercage 13 Å are calculated to be $0.9, 1.8$, and 3.0 eV, respectively, as shown in Fig. 3. Energies of $1s$ and $1p$ states with the diameter of β cage 7 Å are calculated to be 3.1 and 6.3 eV, respectively. Supercages and β cages in zeolite LSX do not have an inversion symmetry at each center of cage. Hence, $1s, 1p$, and $1d$ states hybridize with each other. At low loading densities, s electrons occupy $1s$ - and $1p$ -like states in supercages, because the energies of

quantum states in a larger cage (supercage) are lower than those in a smaller cage (β cage). Near the saturation condition at ambient pressure, $n \approx 9$, s electrons occupy the $1s$ -like states of β cages as well as the $1s$ - and $1p$ -like states of supercages. s electrons in β cages have localized magnetic moments by the single occupancy condition for the $1s$ -like states. The magnetic sublattices at β cages have an antiferromagnetic interaction with the itinerant-electron ferromagnet network at supercages [1,13]. The Curie constant exceeding 100% value of spin $s = 1/2$ as shown in Fig. 7 is explained by the distribution of magnetic moments at both β cages and supercages. By the pressure loading up to 0.3 GPa, the Curie constant gradually decreases as shown in Fig. 7, and the ferrimagnetic properties disappear above 0.4 GPa as shown in Fig. 6. This behavior can be explained by the disappearance of the magnetic sublattice at β cages due to the formation of spin-singlet states by the double occupancy of s electrons at $1s$ -like states of β cages, which leads the magnetic sublattice at supercages to be unstable. The occupation of s electrons at $1p$ -like states in β cages is considered to be difficult, because the energy, 6.3 eV, is much higher than that of $1d$ state in the supercage, 3.0 eV.

The loading density of the K atom at $P \approx 0.9$ GPa where a ferromagnetism appears (see Fig. 6) corresponds to $n \approx 15$ (see Fig. 8). Two of them may fully occupy the $1s$ -like state in the β cage. Thirteen of them fully occupy $1s$ - and $1p$ -like states and partly occupy the $1d$ -like state in the supercage. The Fermi energy is expected to be located at the energy band of the partly filled $1d$ -like states in supercages.

1. Stoner model

According to the Stoner model of itinerant electron ferromagnetism, the ferromagnetic state at 0 K occurs under the Stoner condition

$$\frac{UD(E_F)}{N} > 1, \quad (5)$$

where $D(E_F)$ is the DOS at the Fermi energy E_F , and N is the number of sites. $D(E_F)$ at ferromagnetic loading pressure ≈ 0.9 GPa is estimated to be $D(E_F)/N \approx 46$ states/eV per cage, which is about five times larger than that in bulk K metal ≈ 10 states/eV. The unscreened U is estimated to be ≈ 3 eV at the supercage with the inside diameter 13 Å [1]. In general, the Curie temperature expected from the Stoner model in Eq. (5) is too high. The electron correlation in the narrow band, however, is known to reduce U to the order of the bandwidth, when U is much larger than the bandwidth [32]. In this sense, U should be replaced by the effective energy U_{eff} . According to this calculation, the ferromagnetic condition cannot be satisfied easily in a simple band structure [32].

In addition to the above theory, the orbital degeneracy stabilizes an itinerant-electron ferromagnetism [33–38]. In the present system, the $1d$ -like state in the supercage is expected to have an orbital angular momentum. A remarkable enhancement of spin-orbit interaction in the partly filled $1d$ -like state at the supercage is expected, similarly to the Rashba mechanism in the $1p$ -like state [1,7]. Furthermore, flat bands in the Weaire-Thorpe model [39] are expected to enhance the stability of an itinerant electron ferromagnetism in zeolite LSX with

a diamond structure. Actually, the energy bandwidth of peak at 0.96 GPa in Fig. 8(a), which is estimated to be ≈ 0.04 eV in Sec. III B, is very narrow. The orbital degeneracy and the flat bands may contribute to U_{eff} and $D(E_F)$, and stabilize the ferromagnetism at ≈ 0.9 GPa. Numerical estimations are quite important, but they are future works of theoretical calculations in relevant systems. Anyway, it is concluded from the present experimental results that the ferromagnetism at ≈ 0.9 GPa satisfies the ferromagnetic condition

$$\frac{U_{\text{eff}}D(E_F)}{N} > 1. \quad (6)$$

2. Revised Rhodes-Wohlfarth plot

The Curie-Weiss law observed in metals is not explained by the Stoner model. The self-consistent renormalization (SCR) theory has been developed by the consideration of dynamical spin fluctuation [40]. The Curie-Weiss law has been explained successfully by the SCR theory. A revised Rhodes-Wohlfarth plot for itinerant electron ferromagnets has given a unified relation between p_{eff}/p_s and T_C/T_0 as [41–43]

$$\frac{p_{\text{eff}}}{p_s} \approx 1.4 \left(\frac{T_C}{T_0} \right)^{-2/3}, \quad (7)$$

instead of the phenomenological Rhodes-Wohlfarth plot between p_{eff}/p_s and T_C [44], where $p_s \mu_B$ is the magnetic moment per site given by the spontaneous magnetization, and $p_{\text{eff}} \mu_B$ the localized magnetic moment estimated from the Curie constant. T_0 is the characteristic temperature corresponding to the energy width of spin fluctuations. This theory can deal with itinerant electron ferromagnetism widely from the Pauli paramagnetic limit (weak ferromagnetism) for $p_{\text{eff}}/p_s \gg 1$ to the localized-moment limit for $p_{\text{eff}}/p_s \approx 1$.

According to the theory of the revised Rhodes-Wohlfarth plot [42], the solution for magnetization M under magnetic field H at $T = 0$ K is given by

$$\begin{aligned} -2c_{4/3} \left(\frac{T_C}{T_0} \right)^{4/3} k_B T_A \frac{M}{\mu_B N_0} \\ + \frac{1}{8} \frac{4k_B T_A^2}{15T_0} \left(\frac{M}{\mu_B N_0} \right)^3 = 2\mu_B H, \end{aligned} \quad (8)$$

where k_B , N_0 , and $k_B T_A$ are the Boltzmann constant, the number of magnetic sites (cages) per unit volume, and the dispersion energy of the static magnetic susceptibility in wave vector space, respectively, and $c_{4/3} = 0.3353$. In the original equation of the theory of the revised Rhodes-Wohlfarth plot in Ref. [42], the magnetization is given by $M/2\mu_B$. In the present paper, M is given in units of G, as in Ref. [45]. Equation (8) is rewritten as

$$M^2 = \frac{16\mu_B^4 N_0^3}{\bar{F}_1} \frac{H}{M} + M_s^2, \quad (9)$$

where

$$\bar{F}_1 = \frac{4k_B T_A^2}{15T_0}, \quad (10)$$

and the spontaneous magnetization M_s is given as

$$M_s^2 = \frac{60T_0 c_{4/3} \mu_B^2 N_0^2}{T_A} \left(\frac{T_C}{T_0} \right)^{4/3}. \quad (11)$$

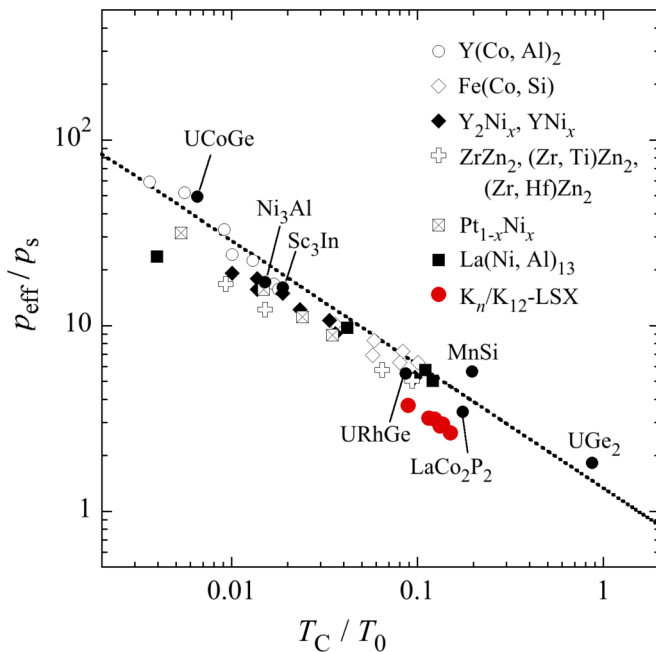


FIG. 11. The theory of the revised Rhodes-Wohlfarth plot (dotted line) and data of K_n/K_{12} -LSX under various loading pressures (red circles). Experimental values for various itinerant electron ferromagnets [43] are also plotted.

Equation (9) has the form of the Arrott plot. The parameter \bar{F}_1 can be experimentally determined from the slope of the Arrott plot. The dimensionless quantity p_s is defined as

$$p_s = \frac{M_s}{\mu_B N_0}, \quad (12)$$

and given by

$$\frac{p_s^2}{4} = \frac{15T_0 c_{4/3}}{T_A} \left(\frac{T_C}{T_0} \right)^{4/3}. \quad (13)$$

Finally the following relation is obtained:

$$\left(\frac{T_C}{T_0} \right)^{5/6} = \frac{p_s^2}{8\sqrt{15}c_{4/3}} \sqrt{\frac{\bar{F}_1}{k_B T_C}}. \quad (14)$$

The parameter T_0 can be experimentally determined by \bar{F}_1 , T_C , and p_s with this equation.

We apply the above-mentioned theory, and estimate ferromagnetic parameters for K_n/K_{12} -LSX. For example, the slope of the Arrott plot at 0.91 GPa is

$$\frac{16\mu_B^4 N_0^3}{\bar{F}_1} \approx 6.9 \times 10^{-5} \text{ G}^3/\text{Oe}, \quad (15)$$

and $\bar{F}_1/k_B \approx 1.7 \times 10^3$ K, $p_{\text{eff}}/p_s \approx 2.64$ and $T_C/T_0 \approx 0.15$ are derived from \bar{F}_1 and other parameters: $T_C = 10.8$ K, $p_s = 0.39$, and $p_{\text{eff}} = 1.1$. Ferromagnetic relations between

p_{eff}/p_s and T_C/T_0 around 0.9 GPa are plotted in Fig. 11 by red circles. The revised Rhodes-Wohlfarth plot given by Eq. (7) is indicated by a dotted line. A close relation to the revised Rhodes-Wohlfarth plot is seen. Experimental values for various itinerant electron ferromagnets [43] are also plotted in Fig. 11. The present result in K_n/K_{12} -LSX around 0.9 GPa is rather near the localized-moment limit of itinerant-electron ferromagnetism.

In the U/t -dominant system with $S = 0$, an antiferromagnetism of the Mott insulator is stabilized theoretically at the just half-filled electron density [46]. Actually, alkali-metal clusters arrayed in a body-centered-cubic structure in zeolite sodalite display a typical Heisenberg antiferromagnetism of Mott insulator at $n = 1$, which corresponds to the just half-filled condition of $1s$ states in β -cage clusters [1,4,14,15,47]. The magnetic moments are well localized in β -cage clusters. In addition to the large U/t , the large S/t at $U > S$ partly contributes to the localization of s electrons [19]. In the present result in K_n/K_{12} -LSX around 0.9 GPa, an intermediate U/t with a small S/t may be realized by the increase in t , because of large windows of $8R$'s of supercages and higher quantum states. An itinerant-electron system with nearly localized magnetic moments for s electrons is generated in partly filled $1d$ -like states at $n \approx 15$, where 13 s electrons occupy $1s-1p-1d$ -like states in each supercage cluster and two s electrons fully occupy a $1s$ -like state in each β -cage cluster. Finally, the itinerant electron ferromagnetism may be stabilized at low temperatures by the assistance of the orbital degeneracy and the flat bands in $1d$ -like states.

IV. SUMMARY

K metal is successfully loaded into regular nanospaces of zeolite K_{12} -LSX by the pressure-loading technique. The loading density of K atoms per cage n is increased from 9.1 at ambient pressure up to 17 at 1.5 GPa. With the loading pressure, ferrimagnetic properties observed at ambient pressure disappear at ≈ 0.3 GPa, and a new ferromagnetism is observed at ≈ 0.9 GPa. Properties of the ferromagnetism are analyzed in terms of the Stoner condition and the revised Rhodes-Wohlfarth plot.

ACKNOWLEDGMENTS

The authors would like to thank Professor T. Kagayama for her advice on the pressure experiments, and also thank Professor R. Arita and Professor H. Aoki for their critical comments on this work. This work was partially supported by Grant-in-Aid for Scientific Research (A) (Grants No. 24244059 and No. 13304027), a Grant-in-Aid for Scientific Research on Priority Areas (Grant No. 19051009) from MEXT Japan, and also by the Global COE Program ‘‘Core Research and Engineering of Advanced Materials-Interdisciplinary Education Center for Materials Science,’’ MEXT Japan.

[1] T. Nakano and Y. Nozue, *Adv. Phys.: X* **2**, 254 (2017).

[2] Y. Nozue, T. Kodaira, and T. Goto, *Phys. Rev. Lett.* **68**, 3789 (1992).

[3] Y. Nozue, T. Kodaira, S. Ohwashi, T. Goto, and O. Terasaki, *Phys. Rev. B* **48**, 12253 (1993).

[4] V. I. Srdanov, G. D. Stucky, E. Lippmaa, and G. Engelhardt, *Phys. Rev. Lett.* **80**, 2449 (1998).

- [5] T. Nakano, Y. Ikemoto, and Y. Nozue, *Eur. Phys. J. D* **9**, 505 (1999).
- [6] T. Nakano, D. Kiniwa, Y. Ikemoto, and Y. Nozue, *J. Magn. Magn. Mater.* **272-276**, 114 (2004).
- [7] T. Nakano and Y. Nozue, *J. Comput. Methods Sci. Eng.* **7**, 443 (2007).
- [8] T. C. Duan, T. Nakano, and Y. Nozue, *J. Magn. Magn. Mater.* **310**, 1013 (2007).
- [9] N. H. Nam, S. Araki, H. Shiraga, S. Kawasaki, and Y. Nozue, *J. Magn. Magn. Mater.* **310**, 1016 (2007).
- [10] N. H. Nam, T. Ohtsu, T. Araki, S. Araki, and Y. Nozue, *J. Phys.: Conf. Ser.* **200**, 012062 (2010).
- [11] D. T. Hanh, T. Nakano, and Y. Nozue, *J. Phys. Chem. Solids* **71**, 677 (2010).
- [12] T. Nakano, D. T. Hanh, Y. Nozue, N. H. Nam, T. C. Duan, and S. Araki, *J. Korean Phys. Soc.* **63**, 699 (2013).
- [13] T. Nakano, D. T. Hanh, A. Owaki, Y. Nozue, N. H. Nam, and S. Araki, *J. Korean Phys. Soc.* **63**, 512 (2013).
- [14] T. Nakano, Y. Ishida, A. Hanazawa, and Y. Nozue, *J. Korean Phys. Soc.* **62**, 2197 (2013).
- [15] T. Nakano, H. Tsugeno, A. Hanazawa, T. Kashiwagi, Y. Nozue, and M. Hagiwara, *Phys. Rev. B* **88**, 174401 (2013).
- [16] L. M. Kien, T. Goto, D. T. Hanh, T. Nakano, and Y. Nozue, *J. Phys. Soc. Jpn.* **84**, 064718 (2015).
- [17] H. Aoki, *Appl. Surf. Sci.* **237**, 2 (2004).
- [18] R. Arita, T. Miyake, T. Kotani, M. van Schilfgaarde, T. Oka, K. Kuroki, Y. Nozue, and H. Aoki, *Phys. Rev. B* **69**, 195106 (2004).
- [19] Y. Shinozuka, *J. Phys. Soc. Jpn.* **56**, 4477 (1987).
- [20] P. W. Anderson, *Phys. Rev. Lett.* **34**, 953 (1975).
- [21] P. T. Thi, T. Nakano, Y. Sakamoto, and Y. Nozue, *J. Phys. Soc. Jpn.* **85**, 024703 (2016).
- [22] P. T. Thi, T. Nakano, Y. Sakamoto, and Y. Nozue, *IOP Conf. Ser.: Mater. Sci. Eng.* **196**, 012002 (2017).
- [23] International Zeolite Association (IZA), available at <http://www.iza-online.org>.
- [24] T. Ikeda, T. Nakano, and Y. Nozue, *J. Phys. Chem. C* **118**, 23202 (2014).
- [25] C. J. Pickard and R. J. Needs, *Phys. Rev. Lett.* **107**, 087201 (2011).
- [26] G. Fabbris, J. Lim, L. S. I. Veiga, D. Haskel, and J. S. Schilling, *Phys. Rev. B* **91**, 085111 (2015).
- [27] A. K. Kuriakose and E. Whalley, *J. Chem. Phys.* **48**, 2025 (1968).
- [28] L. G. Liu, *J. Phys. Chem. Solids* **47**, 1067 (1986).
- [29] M. Alouani, N. E. Christensen, and K. Syassen, *Phys. Rev. B* **39**, 8096 (1989).
- [30] M. Tanaka, *Prog. Theor. Phys.* **29**, 675 (1963).
- [31] M. Watabe and M. Tanaka, *Prog. Theor. Phys.* **31**, 525 (1964).
- [32] J. Kanamori, *Prog. Theor. Phys.* **30**, 275 (1963).
- [33] Y. Kakehashi, *Phys. Rev. B* **38**, 6928 (1988).
- [34] K. Kusakabe and H. Aoki, *Physica B (Amsterdam)* **194-196**, 217 (1994).
- [35] H. Sakamoto, T. Momoi, and K. Kubo, *Phys. Rev. B* **65**, 224403 (2002).
- [36] K. Kusakabe and H. Aoki, *J. Phys. Soc. Jpn.* **61**, 1165 (1992).
- [37] S. Sakai, R. Arita, and H. Aoki, *Phys. Rev. Lett.* **99**, 216402 (2007).
- [38] Y. Li, E. H. Lieb, and C. Wu, *Phys. Rev. Lett.* **112**, 217201 (2014).
- [39] Y. Hatsugai, K. Shiraishi, and H. Aoki, *New J. Phys.* **17**, 025009 (2015).
- [40] T. Moriya, *J. Magn. Magn. Mater.* **14**, 1 (1979).
- [41] Y. Takahashi and T. Moriya, *J. Phys. Soc. Jpn.* **54**, 1592 (1985).
- [42] Y. Takahashi, *J. Phys. Soc. Jpn.* **55**, 3553 (1986).
- [43] Y. Takahashi, *J. Phys.: Conf. Ser.* **868**, 012002 (2017).
- [44] P. Rhodes and E. P. Wohlfarth, *Proc. R. Soc. London, Ser. A* **273**, 247 (1963).
- [45] K. Shimizu, H. Maruyama, H. Yamazaki, and H. Watanabe, *J. Phys. Soc. Jpn.* **59**, 305 (1990).
- [46] T. Moriya and H. Hasegawa, *J. Phys. Soc. Jpn.* **48**, 1490 (1980).
- [47] K. Nakamura, T. Koretsune, and R. Arita, *Phys. Rev. B* **80**, 174420 (2009).